ABSTRACT

ARCHER, JOHN RICHARD. Multi-objective Design Optimization of a Variable Geometry Spray Fuel Injector. (Under the direction of Gregory D. Buckner.)

This work develops and demonstrates a novel simulation-based design optimization strategy based on multiple performance objectives. While this technique could be applied to a wide range of electromechanical systems, this paper focuses on the optimization of a novel variable geometry spray (VGS) fuel injector. A multi-objective genetic algorithm (MOGA), used to explore the design space for optimality, is interfaced to state-of-the-art multi-physics simulators to optimize the design of this inherently nonlinear system. Commercial computational fluid dynamics (CFD) software is used to predict the spray characteristics of each VGS candidate design; other computational tools are used to evaluate the performance objectives and update the design parameters. The entire design process is parallelized using a high performance Linux blade cluster, significantly enhancing the computational performance. The MOGA creates a Pareto frontier of optimal designs, which clearly reveals the inherent tradeoff between performance objectives. The MOGA also results provide insight into the dependencies between design parameters and performance objectives; valuable design information for the continued development of this VGS technology.

Multi-objective Design Optimization of a Variable Geometry Spray Fuel Injector

by
John Richard Archer

A thesis submitted to the Graduate Faculty of
North Carolina State University
in partial fulfillment of the
requirements for the degree of
Master of Science

Mechanical Engineering

Raleigh, North Carolina

2013

APPROVED BY:

_____	_____
Scott M. Ferguson	Gary W. Howell
_____	_____
Tiegang Fang	Gregory D. Buckner Committee Chair

DEDICATION

To my Lord and Savior Jesus Christ

BIOGRAPHY

The author was born in Altamonte Springs, Florida, raised in Boone, North Carolina, and graduated from Watauga High School in 2007. He attended Appalachian State University from 2007-2011 where he earned a degree in Applied Physics. While at Appalachian State, he played varsity basketball all four years. Since 2011 he has been a student in the Mechanical and Aerospace Engineering department at North Carolina State University. He has accepted an offer of employment with Harris Corporation.

ACKNOWLEDGMENTS

A number of people provided a valuable support on this project:

My adviser, Dr. Buckner, has spent more hours on this project than anyone besides myself, and his guidance shaped it from the original concept through the final edits. I will always be grateful for the time he spent teaching me to write and present information more effectively.

The members of my committee were always generous with their time and ideas throughout this research. Each provided valuable ideas and advice in their own areas of expertise. I am grateful to the National Science Foundation for funding my work on this project through the Combustion, Fire, and Plasma Systems program.

All of the researchers in the EMRL helped in various ways throughout the process. J.P. Lien helped me get going as I picked up this project. Casey Haigh always let me bounce ideas off him and Andy Richards was a great source of information through the process. Shaphan Jernigan always helped me find what I needed in the lab.

Skip Richardson did an awesome job building the prototypes and making modifications to overcome unforeseen problems.

Priyesh Sharma of Dr. Fang's lab was very accommodating and helpful as we shared the same experimental setup.

I want to thank my friends, family, and especially my parents John and Lisa Archer, who provided endless moral support through the ups and downs of the research process.

Finally, I am eternally grateful to my Lord and Savior Jesus Christ who carried me every step of the way.

TABLE OF CONTENTS

LIST OF TABLES

LIST OF FIGURES

1 INTRODUCTION

The design, fabrication, and experimental evaluation of sophisticated electromechanical systems can be a time-consuming and expensive process. Inherent non-linearities (flux saturation, flux hysteresis, hardening springs, etc.) necessitate the need for an iterative design and fabrication approach. Optimizing the design of such systems, which may have large numbers of critical design parameters and multiple conflicting performance objectives, can significantly hinder the development and commercialization of innovative technologies. This is particularly true in academic research environments, where facilities and financial resources are limited.

One such technology, variable-geometry spray (VGS) fuel injection, has the potential to significantly improve the efficiency of internal combustion engines while simultaneously reducing emissions. This patent-pending technology enables independent control of fuel flow rate and spray geometry as it enters the combustion chamber. By optimizing air-fuel mixing and the distribution of atomized fuel within the cylinder, VGS injection has the potential to enable combustion at peak efficiency, maximizing power output.

With limited R&D resources, three generations of VGS fuel injector prototypes were developed, and preliminary results with low-pressure working fluids were very encouraging. However, because each prototype required approximately 25,000 man hours to fully design, fabricate and experimentally evaluate, most of the design space remained unexplored and little was known regarding the effects of critical design parameters on fuel spray characteristics. Investigating the design space for optimal spray performance using this ad-hoc strategy was an inefficient use of time and financial resources.

The goal of this research was to develop and demonstrate a unique, simulation-based design optimization strategy for a sophisticated electromechanical system: a hollow-cone VGS fuel injector for diesel IC engines. A multiple-objective genetic algorithm (MOGA) was employed to efficiently and thoroughly explore the design space. The MOGA was interfaced to state-of-the-art computational tools, enabling complete performance evaluations in a simulated environment, dramatically enhancing the efficiency of the design process (Fig. 1.1).

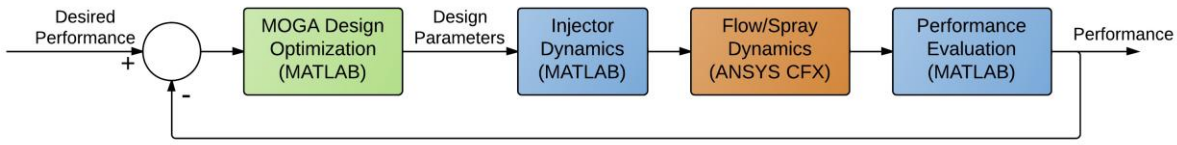

Figure 1.1: Simulation-based design strategy for VGS fuel injector

While the use of computational tools in the design process is not new, this combination of MOGAs interfaced to commercial multi-physics simulators to optimize the design of an inherently nonlinear electromechanical system is innovative. Despite its focus on VGS fuel injection technology, this novel simulation-based design strategy is applicable to a wide range of electromechanical systems, and could enable more efficient and flexible commercialization of innovative technologies.

1.1 Combustion Background

Designers of internal combustion engines face an ongoing and critical need to reduce emissions in order to keep up with increasingly strict regulations. The US Environmental

Protection Agency [1] has set maximum levels for particulate matter (PM, or soot) and nitrogen oxides (NO_x). It is very difficult to meet these requirements using conventional diesel combustion methods. Simultaneous improvements in both of these emissions products have been limited due to the fundamental PM-NO_x tradeoff shown in Fig. 1.2 [2]. In conventional diesel combustion, the reactants are only partially premixed, therefore many reactions take place in fuel-rich regions. Such regions give rise to soot particles due to the scarcity of oxygen. PM can be reduced by increasing combustion temperature in order to promote soot oxidization. However, higher temperatures increase dissociation of diatomic nitrogen ($N_2 \rightarrow 2N$) resulting in increased formation of NO_x.

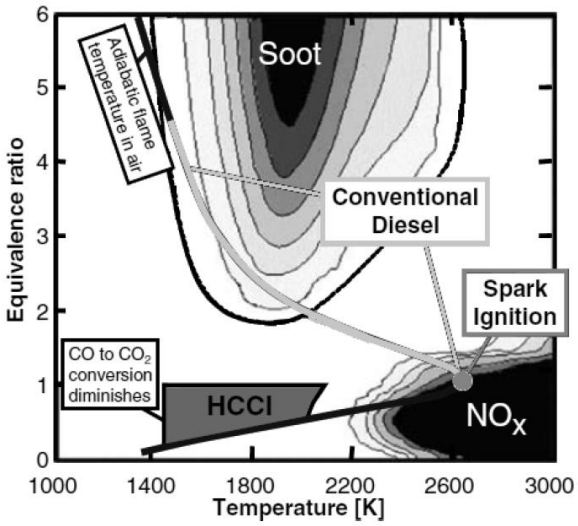

Figure 1.2: Plot of equivalence ratio vs. temperature of combustion, illustrating regions of soot and NO_x formation. Regions corresponding to conventional diesel, spark ignition, and HCCI combustion are highlighted. Adapted from [3]

Homogeneous charge compression ignition (HCCI) is one promising technique to solve the soot-NO_x¬ tradeoff. HCCI is a combustion mode that seeks to attain clean combustion for

a wider range of fuel richness by lowering combustion temperatures (Fig. 1.2). HCCI does this by combining premixed charge (as in spark-ignition engines) with the compression ignition of diesel engines [4]. Despite the surge of HCCI research and development, feasible implementations in diesel engines have yet to be realized. Currently HCCI must use a lean mixture to minimize soot formation, which makes it difficult to achieve power densities that compete with conventional diesel combustion [5]. Dual-mode combustion strategies have been proposed to overcome these challenges. Such techniques use HCCI under partial load conditions and conventional diesel combustion whenever full power is required [6, 7, 8]. This allows for overall reduction of emissions without significant loss in performance, but conventional fuel injectors have fixed spray geometries that are not optimal for all modes [9]. Lowering emissions in multi-mode combustion strategies requires a novel fuel injector capable of varying the spray geometry to be optimal for all modes.

1.2 VGS Prototype Development

For the past three years, our research group has focused on the development of patent-pending variable geometry spray (VGS) fuel injector prototypes, as detailed in Lien, et al [10]. This injector enables continuous control of fuel spray angle, independent of fuel flow rate or other vital injection parameters. As illustrated in Fig. 1.3, the VGS injector is centrally-positioned and the optimal spray angle targets the lip of the piston bowl throughout the compression stroke, thus minimizing liner wetting and fuel impingement. This optimal spray angle trajectory can be readily computed and plotted as a function of engine timing (Fig. 1.4), measured in Crank Angle Degrees (CAD) before top dead center (BTDC).

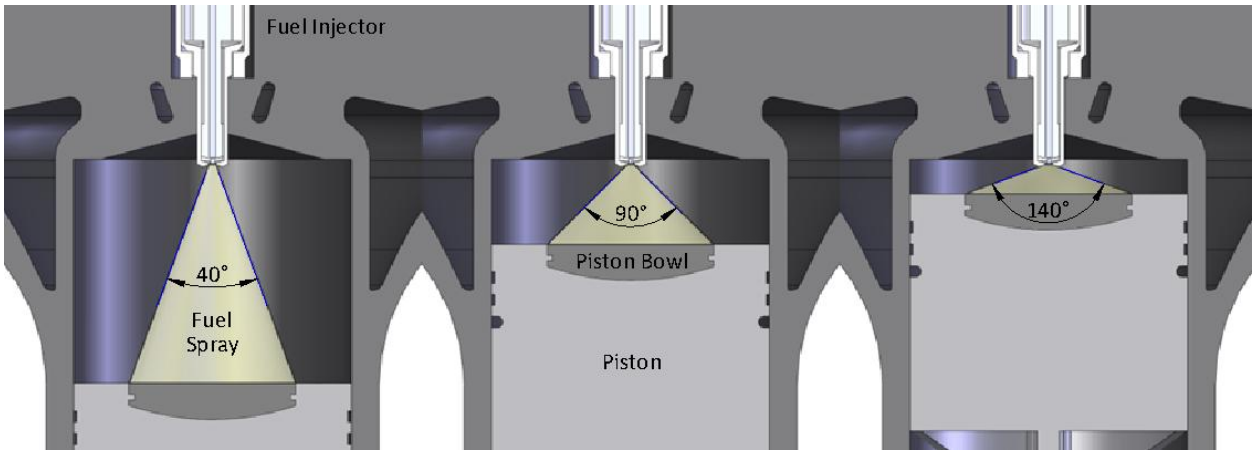

Figure 1.3: VGS fuel injection for optimized combustion: spray angle variation during engine cycle to ensure targeting of piston bowl and avoid liner wetting and fuel impingement.

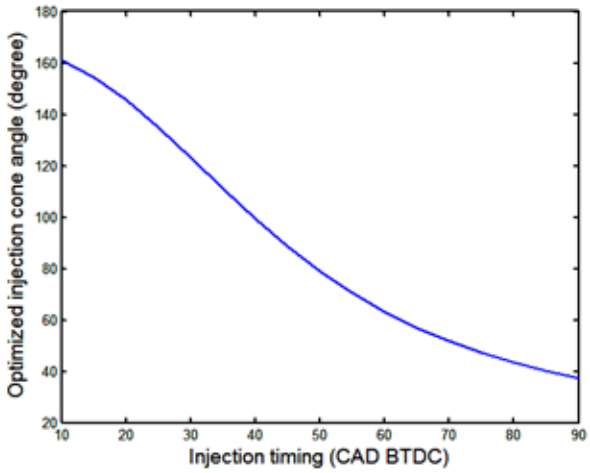

Figure 1.4: Optimal included spray angle as a function of injection timing [11]

While pintle mechanisms have been used in conventional fuel injectors to regulate fuel flow [12], in our VGS design this mechanism is employed to vary the fuel spray angle. When the pintle is fully retracted into the nozzle, the spray cone has a narrow included angle; when fully deployed this angle is significantly increased (Fig. 1.5). By adjusting the position of this

pintle relative to the nozzle orifice, a wide and controllable range of spray angles can be achieved.

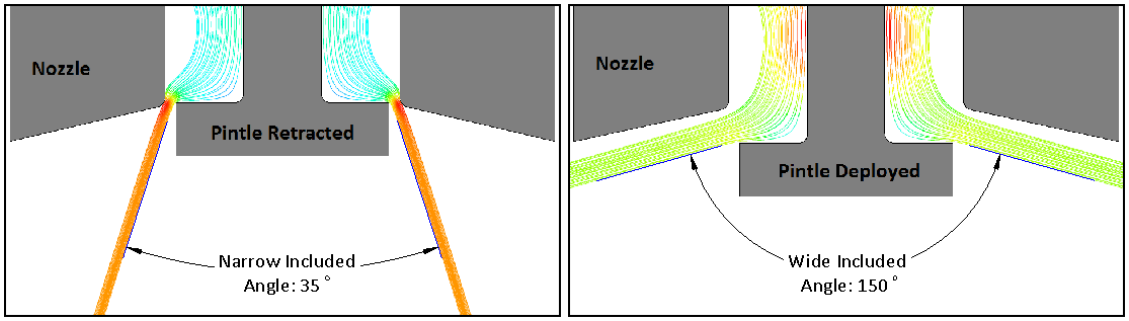

(a) **(b)**

Figure 1.5: 2D simulation results of the VGS fuel injection concept: (a) when the pintle is fully retracted, the fuel spray cone has a narrow included angle; (b) when the pintle is fully deployed, it redirects fuel flow to a significantly wider included angle

To experimentally validate the VGS concept (that included spray angles between 70-150° could be realized by manipulating pintle position), a limited-functionality prototype was fabricated using stereolithography. This low-pressure prototype featured a 200 μm annular gap between the nozzle and pintle, which was manually actuated by turning a screw. Using pressurized water as the working fluid (200-1500 psi), included spray angles were measured using digital image post-processing [11]. Spray angle results for 13 different pintle positions and four operating pressures are presented in Fig. 1.6. While this preliminary prototype validated a repeatable and significant dependence of spray angle on pintle position, it had several notable limitations. Obviously, the screw mechanism for adjusting pintle position did not allow for electronic actuation or dynamic spray testing. Also the geometry, dimensions, materials and working fluid of the prototype did not conform to those of conventional common rail fuel injectors. The range of included spray angles (2-93°) was not consistent

with the design requirements (70-150°), and the total pintle displacement (750 μm) was larger than desired. Because of its unconventionally large annular gap (200 μm) and low operating pressures, the prototype's average spray droplet size (as measured using a Malvern Spraytec spray particle analyzer [13]) was approximately five times larger than that of conventional injectors. The Sauter Mean Diameter (SMD) of droplets should be less than 50 μm, as emissions are known to correlate with spray droplet size [14].

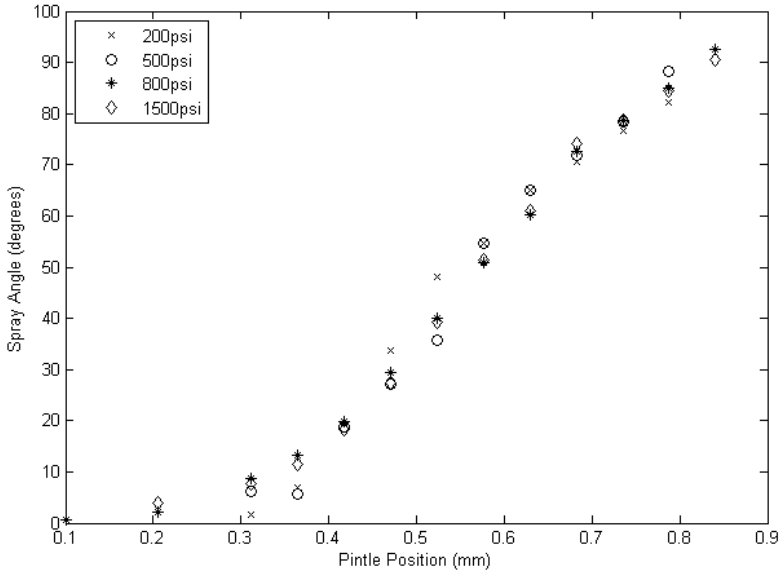

Figure 1.6: Experimental results from manually actuated VGS prototype demonstrating dependence of included spray angle on pintle position

A second prototype was designed to overcome many of these functional limitations. To achieve smaller droplet sizes, the pintle diameter and annular gap were reduced to 1.5mm and 100μm, respectively, based on component measurements from conventional diesel injectors [15].The external nozzle dimensions were chosen to be consistent with "P-type" common rail fuel injectors. The manual actuation screw was replaced by a piezoceramic

stack actuator, and a closed loop pintle displacement control system was implemented. A solenoid valve was integrated to enable electronic regulation of working fluid flow. The spray angles were measured experimentally using water pressurized to 500psi, 1000psi, and 1500psi (Fig. 1.7), and these experiments demonstrated an increase in the range of spray angles (12-140°) with reduced pintle displacement (450 μm). Droplet size measurements for the second generation prototype were small enough to meet the secondary design objectives [11]. Archer et al. [16] describes how the pintle position was dynamically controlled to achieve desired spray angles at bandwidths of up to 20Hz.

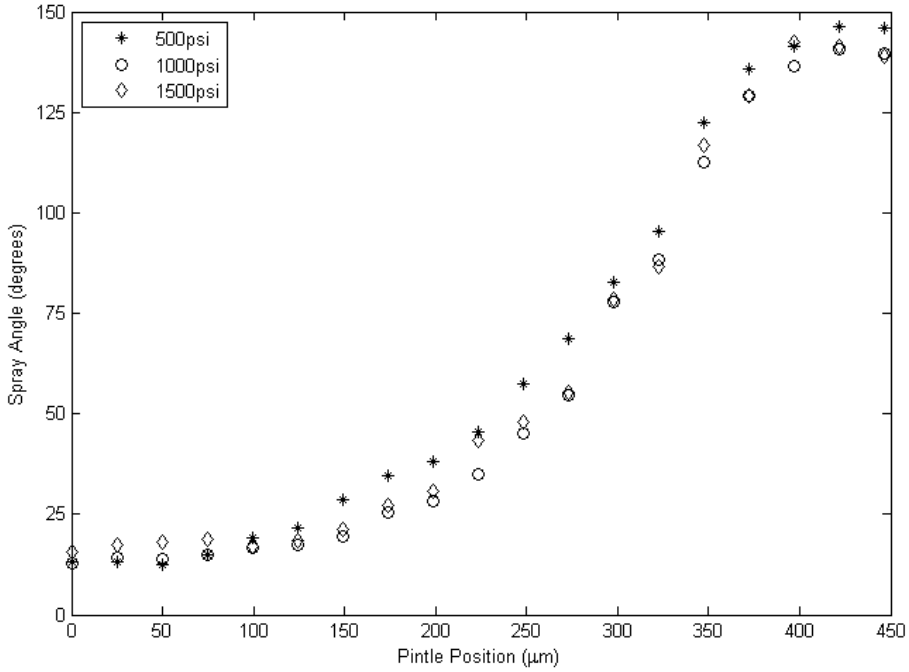

Figure 1.7: Experimental results from second generation prototype demonstrating increased range of included spray angles with decreased pintle displacement

While the second prototype demonstrated a wider range of spray angles with reduced pintle displacement, the external solenoid used to regulate flow was inadequate for actual engine applications. When this solenoid was deactivated, a finite volume of working fluid remained in the channel between the solenoid and the injector nozzle. This fluid drained out of the injector at such low pressures and velocities that it did not atomize; such non-atomized flow would result in unacceptable emission levels in an actual engine.

To minimize concerns with low pressure fluid drainage, a third-generation prototype was designed to regulate fuel flow closer to the nozzle (Fig. 1.8). Conventional common rail injectors (Fig. 1.9) accomplish this objective using nozzle needles [17]. In its deactivated state, the nozzle needle 36 shuts off the flow by blocking the injection holes 46 as it is pressed against the needle seat 45. In its activated state, the nozzle needle is lifted up to allow fluid to flow out of the injection holes. The third-generation VGS prototype (Fig. 1.10) incorporated an annular nozzle needle to accommodate the centrally-located pintle. This nozzle needle was electromechanically actuated in similar fashion to conventional common rail injectors, described in detail by Fujii [17]. Due to limitations in the precision of our fabrication processes, an O-ring was incorporated to seal the nozzle (Fig. 1.10). Experimental testing confirmed the reduction of post-injection fluid drainage. However, movement of this O-ring at high fuel pressures and flow rates interfered with nozzle needle translation and the injector could not be properly activated. Higher precision fabrication techniques are needed for future prototypes to eliminate the need for this O-ring.

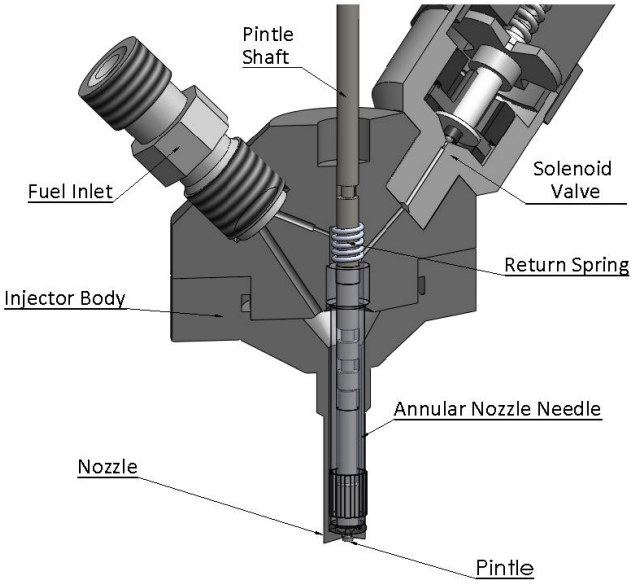

Figure 1.8: Solid model cross-section of third generation VGS prototype, showing annular nozzle needle for regulation of flow

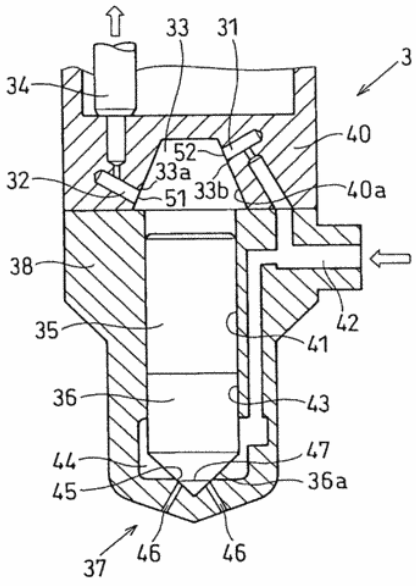

Figure 1.9: Representative cross section of a traditional common rail diesel injector in its deactivated state, where the nozzle needle **36** blocks the injection holes **46** [17]

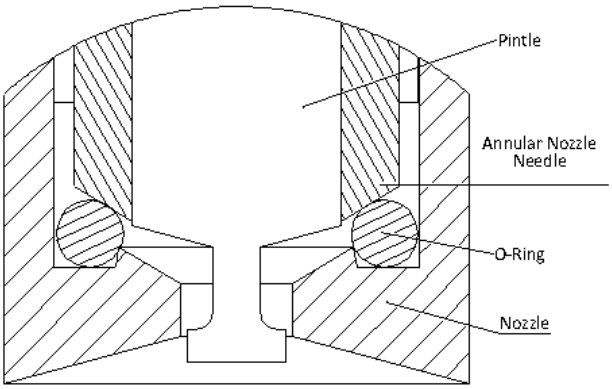

Figure 1.10: Cross section of the distal portion of the third-generation VGS prototype, showing the annular nozzle needle pressed against the O-ring to block flow

2 METHODS

This ad hoc strategy of designing, fabricating, and testing VGS prototypes with limited fabrication resources and precision is time-consuming, expensive, and far from optimal: three years of research and development produced only three functional VGS prototypes, none optimized for implementation in a real IC engine. To fully explore the design space and investigate the dependence of fuel spray angle and droplet size on multiple design parameters required the development of a simulation-based design optimization process.

2.1 Computational Fluid Dynamics

To implement the simulation-based design optimization strategy, it was necessary to accurately and efficiently simulate fuel spray characteristics for candidate VGS design dimensions, flow conditions and pintle displacements. Computational fluid dynamics (CFD) packages provide this capability, using sophisticated meshing algorithms to discretize the fuel flow regime into finite elements, and iterative numerical methods to solve the

differential equations that govern the fluid mechanics. Of the variety of commercial CFD packages available, ANSYS CFX [18] was selected for this application because of its batch mode capabilities and academic license availability. ANSYS CFX runs in the ANSYS Workbench environment, which facilitates the computational modeling and allows batch mode processing using a programming language called Python. Workbench scripts fully automate the analysis tasks associated with each CFD model: varying the model geometry, generating the mesh, applying the boundary conditions, iteratively solving flow equations, and processing the simulation results. These Python scripts offer the advantage that they can be executed by any software application navigating the design space.

In order to optimize computational efficiency, two-dimensional (2D) axisymmetric models (Fig. 2.1) were used, as they exploited the azimuthal symmetry of each fuel spray case. Unstructured, triangular meshes (Fig. 2.1a) were employed to map the curved surfaces of the flow domain and maintain consistent element sizes across the domain [19]. A steady state, two-phase CFD analysis was performed on the flow domain, where the fluid volume initially contained only air at standard temperature and pressure (STP). Because of its similarity to diesel fuel and its regular use in fuel injection testing, Cetane ($C_{16}H_{34}$) with a unit volume fraction served as the working fluid in all CFD simulations. The specified boundary conditions (Fig. 2.1b) were (a) a fuel inlet velocity of 1m/s, (b) a relative combustion chamber pressure of zero, and (c) all pintle and nozzle surfaces are no-slip boundaries. The associated fuel pressures used in CFD analyses were 14.5psi, far below the actual engine operating pressures. These lower fuel pressures were used for CFD analysis because (1) simulating with elevated operating pressures significantly increases the

computational burden (resulting in convergence times greater than 24 hours per case), and (2) experimentally-measured spray angles using VGS prototypes have shown very little dependence on operating pressure (Fig. 1.7).

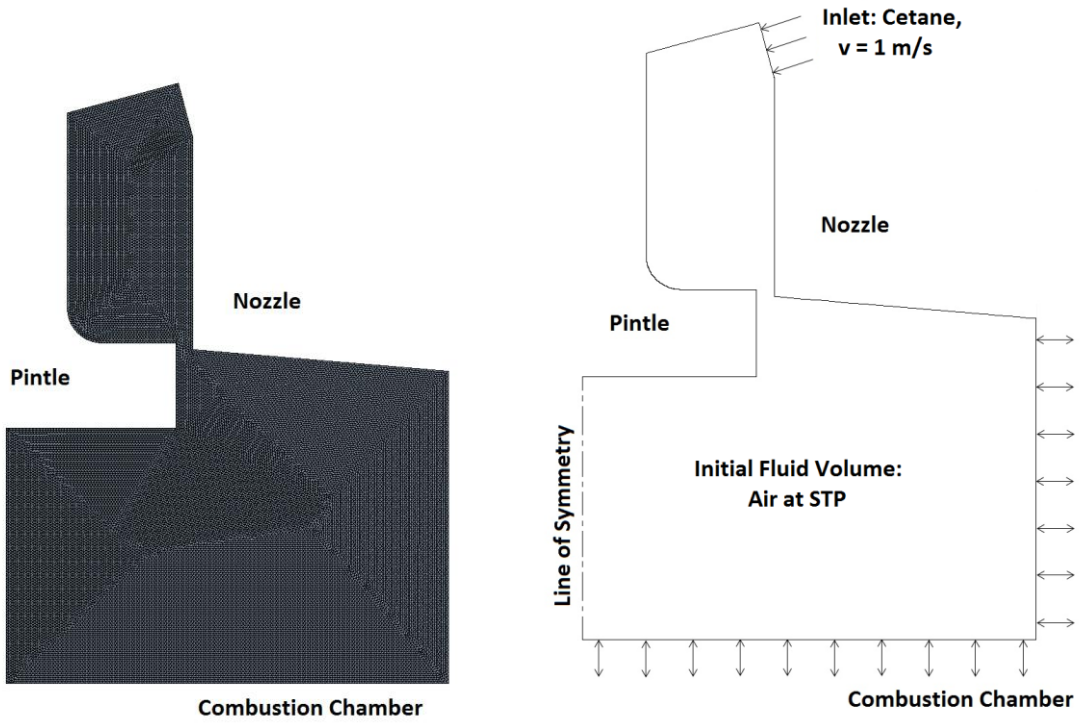

Figure 2.1: 2D axisymmetric model of the fuel flow domain for a candidate VGS design showing: (a) an unstructured triangular mesh and (b) boundary conditions and domain initialization

For each candidate VGS design, nine CFD simulations were performed corresponding to nine pintle displacements (0-400μm) to quantify the relationship between the spray angle and pintle position. To estimate the included spray angle, θ, the following formula was applied to the CFD results using ANSYS CFD-Post:

$$\theta = 2 \cdot \tan^{-1}\left(\frac{x_s - x_p}{y_s - y_p}\right)$$

where x_p, y_p represent the coordinates of the interior corner of the pintle, and x_s, y_s represent the point where the streamlines exit the flow domain (Fig. 2.2).

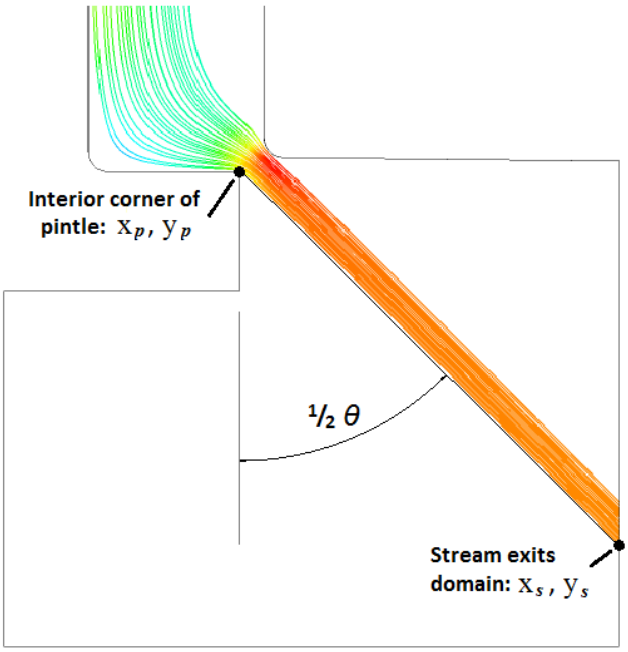

Figure 2.2: CFD results for a candidate VGS design, showing the locations of x_p, y_p and x_s, y_s

To address the inherent tradeoff between computational burden and accuracy, simulations were performed at a variety of different mesh sizes for a given design geometry and boundary conditions. First, an extremely fine mesh (10 μm) was used to solve each domain and determine the resulting spray angle. Subsequent simulations were conducted with linearly increasing mesh sizes, and associated spray angles and convergence times were recorded. Fig. 2.3 quantifies the tradeoff between computational efficiency (convergence time) and accuracy (spray angle error) as functions of mesh size. Based on these results, a standard mesh size of 15 μm was selected for all subsequent simulations because it reduced

computation time by 50% while maintaining an average spray angle error of approximately one degree.

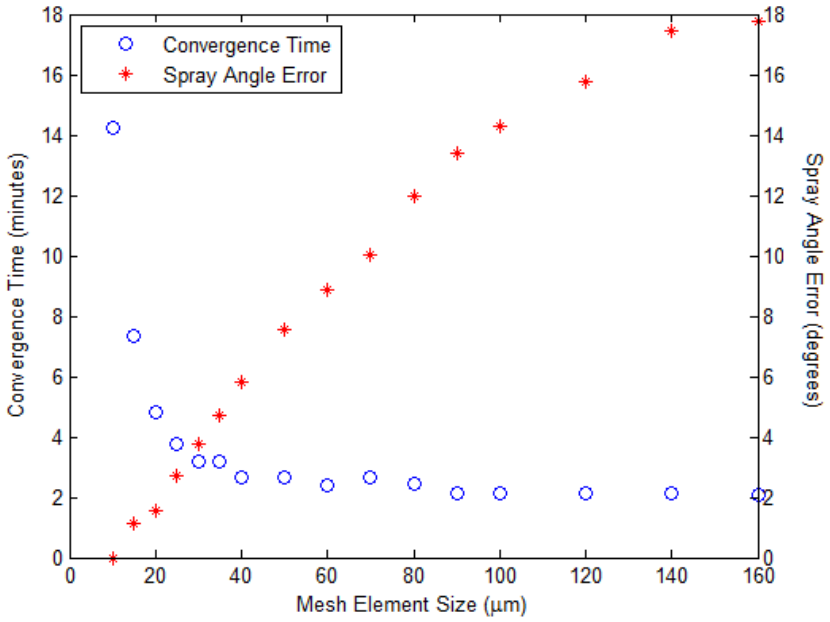

Figure 2.3: Dependence of CFD convergence time and spray angle error on mesh element size, showing the inherent tradeoff between computational efficiency and simulation accuracy

Nonlinear regression was performed on the CFD simulation results from each design case: a hyperbolic tangent curve fit of the nine simulated spray angles was performed on each data set (Fig. 2.4). For cases where one or two of the nine total solutions diverged, regression was performed with these points excluded. If three or more solutions diverged, the design case was discarded.

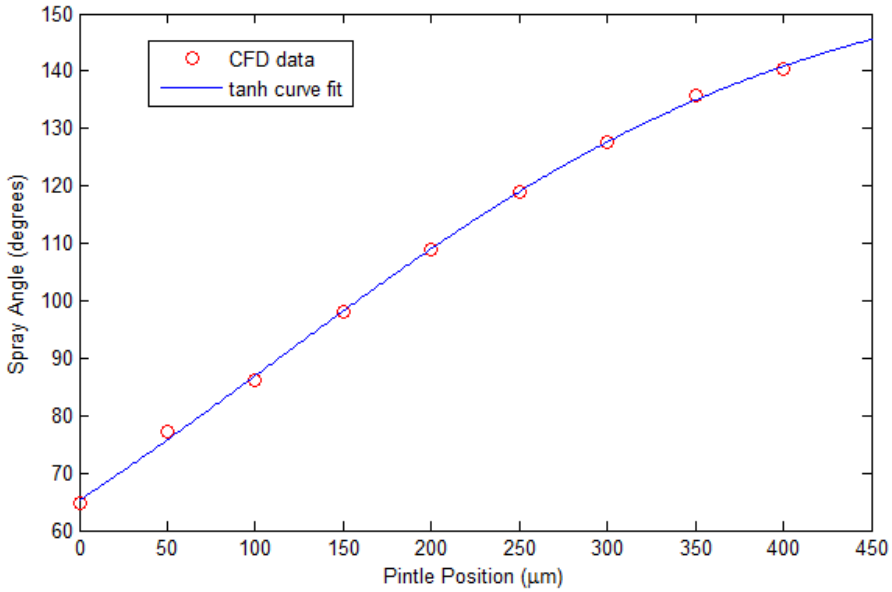

Figure 2.4: Nonlinear regression (hyperbolic tangent) of CFD simulation results (nine different pintle positions) showing dependence of spray angle on pintle position

To validate the accuracy of this CFD modeling approach, experimental spay tests using the second generation VGS prototype were compared to CFD results (Fig. 2.5). Variations in spray angle between the CFD results and experimental measurements are apparent, with an average absolute difference of 9.75°. However, both the mean spray angles (experimental: 72.35°, simulated: 74.34°) and spray ranges (experimental: 131.86° vs. simulated: 125.05°) correlated well enough to justify the use of CFD modeling for the design optimization process.

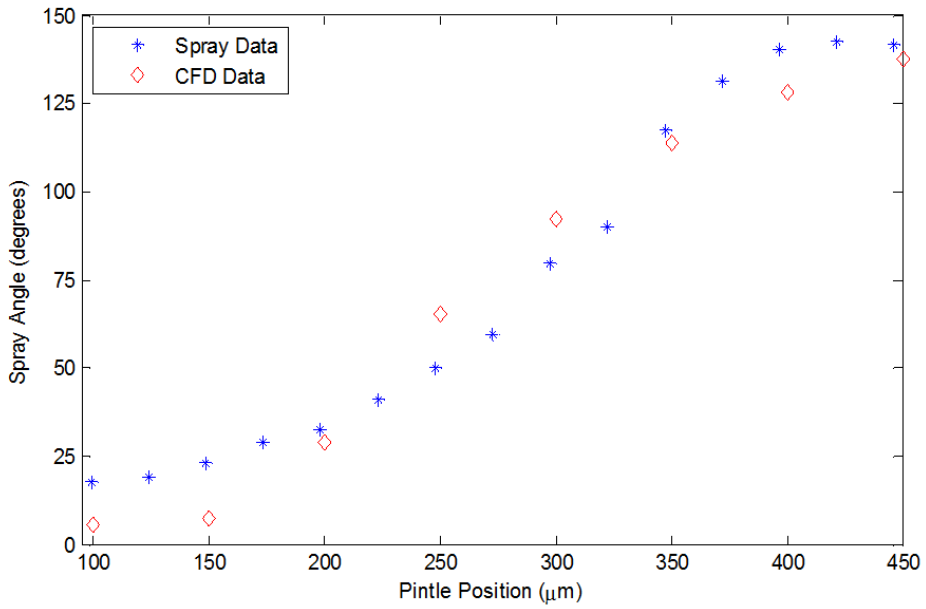

Figure 2.5: Experimental validation of CFD model by comparing CFD results to empirical spray tests for the second generation prototype

2.2 Multi-objective genetic algorithms

Genetic algorithms (GAs) are a class of optimization methods motivated by biological reproduction. GAs seek to minimize or maximize one or more objective functions using computational techniques based on the principles of natural selection [20]. These techniques first create a population of "individuals" (in this case geometric dimensions for the injector). Next "parents" are selected to create "children", and the "fittest" individuals survive (are preserved for use in the next generation). The fitness of an individual is determined using the values of one or more of its objective functions.

There are numerous advantages of using GAs over other optimization techniques. They are zero-order methods, so they rely only on objective function evaluations and require no derivative information. The individuals in the population can be evaluated simultaneously,

which makes it very easy to parallelize objective function evaluations for modern multicore and multi-threaded processors. Furthermore, GAs maintain feasibility for each solution instead of requiring iterative penalty methods. Additionally, they are capable of finding global solutions to optimization problems with multiple local minima [21]. GAs have been applied to a number of interesting design optimization problems, such as trusses [22] active vehicle suspension [23], and a variety of control problems [24-25].

The design and organization of genetic algorithms have been exhaustively studied in the literature [21]. The structure of GAs always contains the following steps: encoding, population initialization, fitness evaluation, parent selection, genetic operators, and termination criterion. Encoding refers to how an individual's design information is represented: binary, discrete, or real valued. The population can be initialized randomly or systematically. Systematic initialization can speed convergence if the investigator has some knowledge of the design space beforehand, but if too small a sample of the design space is used the algorithm may find only local minima and miss the global optimum. While the fitness of a design is often based on the objective functions, more advanced techniques exist to handle multi-objective problems [26]. There are many options and variations for the remaining optimization operators. Parental selection is the process of choosing which of the existing designs will pass on its design information to the next generation. Once parents are selected, they go through crossover (the process of combining the parents to create new children) and mutation (the random change of all or part of an individual's design). Termination criteria are used to determine when the optima have been achieved. The general structure of a GA is shown in Fig. 2.6.

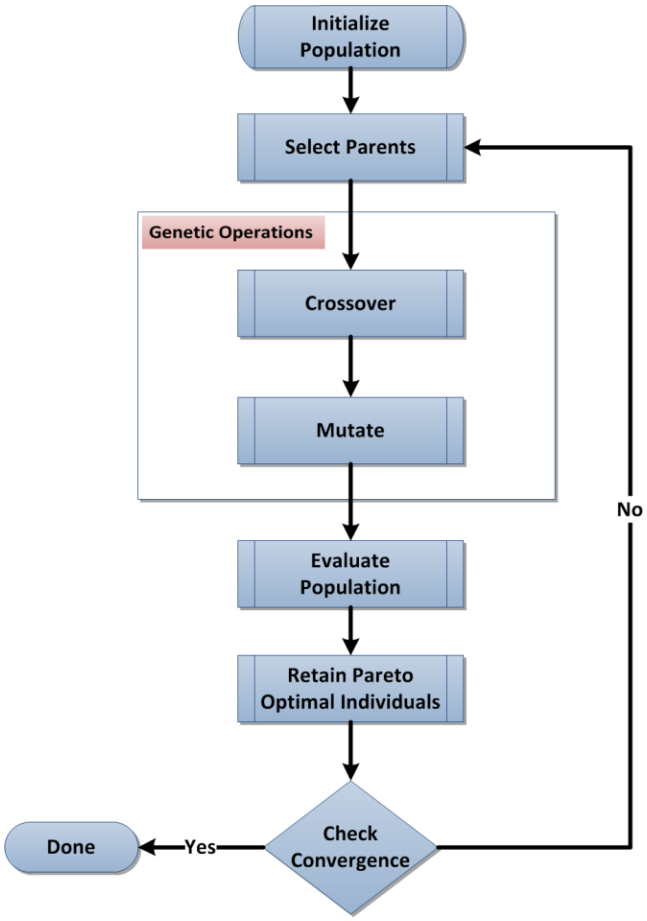

Figure 2.6: Multi-objective Genetic Algorithm flowchart [20]

Multi-objective and single objective optimization problems differ in a number of ways related to fitness evaluation. Single objective optimization algorithms attempt to minimize or maximize a single objective function $F(\mathbf{x})$, where x is an array of the design variables. By contrast, multi-objective optimization problems have solutions that depend on complex interactions between multiple objective functions $F_1(\mathbf{x})$, F_2 $(\mathbf{x})$,.., $F_N(\mathbf{x})$. If simultaneous reductions in all objective functions can be achieved, the objective functions are said to be "cooperative". In these cases the algorithm converges to a single optimal solution. If reductions in one or more objective functions can only be achieved by increases in others, the

objective functions are "conflicting". In these cases a Pareto frontier of non-dominated solutions exists [27]. Both single and multiple objective optimization algorithms can contain equality and inequality constraints on the design variables.

2.2.1 Objective functions

The genetic algorithm seeks to simultaneously minimize the two competing objective functions used in this work: actuator stroke (F_1) and spray angle sensitivity (F_2). The required stroke is directly proportional to the size and cost of the actuator, which should ideally be as small as possible. The spray angle sensitivity, defined as the maximum change in spray angle with respect to pintle position, significantly influences the control challenge as sensitivity is directly proportional to errors in spray angle. Therefore, minimizing actuator stroke and spray angle gain reduces actuator cost and enhances the control system performance.

2.2.1.1 Actuator stroke

The translational motion of the pintle must be actuated at speeds up to about 188Hz [16], and the actuator must be capable of running continuously in an engine environment with minimal power consumption. For these reasons, a piezoelectric actuator was chosen, specifically a PZT stack actuator. Because PZT stack actuators have peak strains of approximately 0.1% [28], a pintle stroke of 100μm would require a 10 cm long PZT stack, much too large for practical implementation in an engine environment. The actuator stroke objective function, F_1, is defined to be:

$$F_1 = x_{150} - x_{70}$$

where x_{150} is the pintle position when the spray angle is 150° and x_{70} is the pintle position when the spray angle is 70°. If a candidate design did not achieve the desired range of spray angles, its objective function was given a penalty proportional to the difference between the desired and achieved range.

2.2.1.2 Spray angle sensitivity

Another important factor in implementing high speed control of the novel injector is the spray angle sensitivity (G_{SA}), which is defined as the change in spray angle ($d\theta$) for a given change in pintle position (dPP), represented in the following equation:

$$G_{SA} = \frac{d\theta}{dPP}$$

Tracking errors in pintle position (e_{PP}) produce tracking errors in spray angle (e_{SA}) via the spray angle sensitivity:

$$e_{SA} = e_{PP} \cdot G_{SA}$$

Because errors in pintle position are inevitable, it is important to minimize spray angle sensitivity. The sensitivity performance objective, F_2, is defined to be:

$$F_2 = max\left\{ i = 2, 3, \dots, n \;\middle|\; \frac{\theta_i - \theta_{i-1}}{y_{p,i} - y_{p,i-1}} \right\}$$

Where θ_i is the spray angle corresponding to the i^{th} pintle position $y_{p,i}$ (of nine total, Fig. 2.4).

2.2.2 Optimization Problem

The two performance objectives described above are competing, because as the required stroke approaches zero the slope approaches infinity, and vice versa. Therefore, the result of optimizing these two performance objectives is a Pareto frontier of non-dominated designs. The theoretical limits of this Pareto frontier can be found by calculating the best possible stroke for each value of spray angle sensitivity. This theoretical limit was used as a representative curve to gauge the performance of the algorithm. Here is the optimization problem in standard form:

$$\begin{aligned} &\text{min} && F_1, F_2 \\ &\text{subject to} && h_k(\vec{u}) = 0, k = 1..K \\ & && g_j(\vec{u}) \leq 0, j = 1..J \end{aligned}$$

The design variables, $\vec{u}$, are geometric dimensions of the pintle and nozzle, and are defined in the following section.

2.3 Design Parameters

The design optimization was limited to only those geometric parameters that had the greatest influence on included spray angle. For the 15 geometric design parameters, $\vec{p}$, that fully define the model (Fig. 2.7), preliminary CFD analyses revealed that only six ($p_1, p_6, p_7, p_9, p_{10}, p_{12}$) had significant influence on spray angle; these were consequently selected as the design variables, $\vec{u}$, for the optimization (Fig. 2.8).

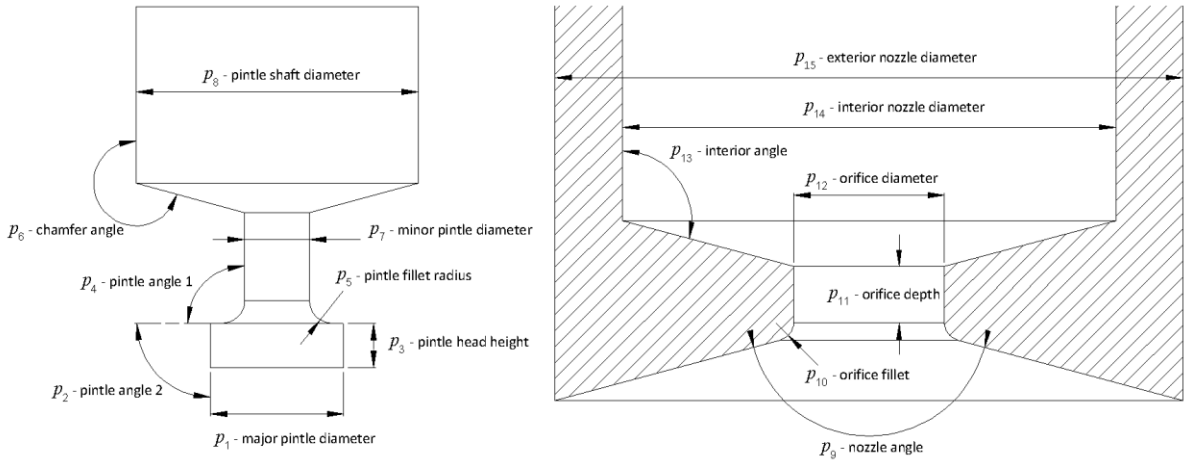

Figure 2.7: The 15 VGS design parameters that fully define the nozzle (left) and the pintle (right)

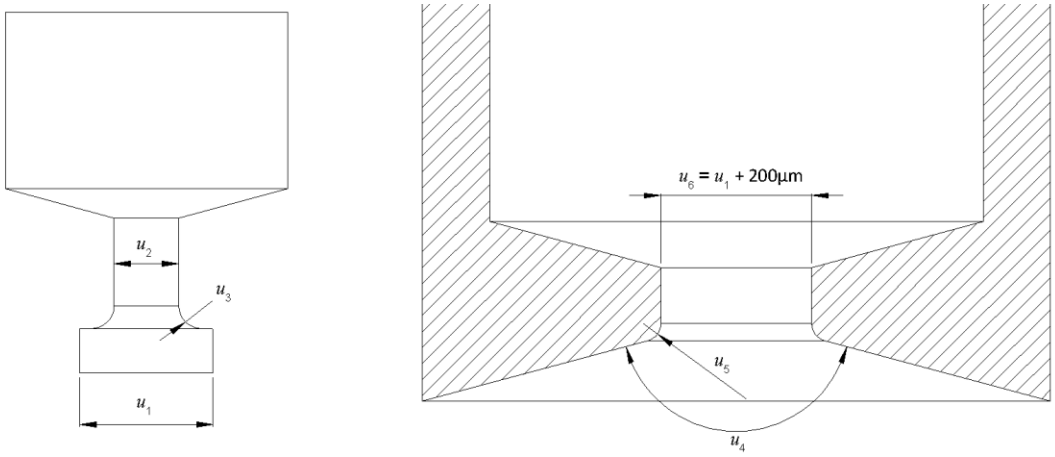

Figure 2.8: The six VGS design variables with the most significant influence on included spray angle, as determined by preliminary CFD analyses: for the nozzle (left) and pintle (right)

Hard geometric constraints were formulated to reject infeasible injector geometries (where, for example, the minor pintle diameter was larger than the major pintle diameter). An equality constraint was placed on the orifice diameter, u_6, (Fig. 2.8) to ensure adequate fuel droplet size (as discussed in Section 1). The constraints are listed below (all units in millimeters unless otherwise noted):

$$1000 \leq u_1 \leq 2000$$
$$400 \leq u_2 \leq 800$$
$$20 \leq u_3 \leq 600$$
$$140° \leq u_4 \leq 180°$$
$$10 \leq u_5 \leq 300$$
$$u_3 + 2 \cdot u_2 \leq u_1$$
$$u_6 = u_1 + 200$$

In addition to constraints on the design variables, constraints were placed on the objective functions so the MOGA would yield only designs with reasonable actuator strokes and spray angle sensitivities. For example, experimental testing with the second generation VGS prototype revealed that peak pintle position errors rarely exceeded 5μm [10], so the maximum spray angle sensitivity was set at 1.5°/μm (corresponding to a peak spray angle error of 7.5°). These performance objective constraints were:

$$F_1 \leq 2000\mu m$$
$$F_2 \leq 1.5\ °/\mu m$$

To provide a balance between robustness and computational efficiency, a population size of 50 was selected and the initial population randomly generated. The top 35% of designs were kept on the Pareto frontier, and of the remaining points 80% were selected for arithmetic crossover. All remaining points were selected for mutation.

2.4 Parallelizing CFD Analysis

Parallel processing techniques were employed to significantly improve computational performance. Using a blade cluster at North Carolina State University's High-Performance Computing (HPC) group, twenty VGS designs could be evaluated simultaneously. This significant improvement in computational performance justified the considerable

programming effort required to automate communication between multiple programs and operating systems.

A powerful freeware scripting engine, AutoIt, was employed to automate communication between MATLAB, ANSYS, and the HPC. (Figs. 2.9 and 2.10). AutoIt programs (1) guided the creation of input files, (2) renamed the input files to designate the appropriate design points and pintle positions, (3) transferred the input files onto the HPC using Secure File Transfer Protocol (SFTP), (4) submitted the jobs to the blade cluster using PuTTY (an open source ssh client), (5) retrieved the output files from the HPC via SFTP, (6) orchestrated the post-processing of results, and (7) determined when a MOGA population was fully evaluated. These Autoit applications were designed to parallelize tasks as much as possible (Fig. 2.10) and to guard against a variety of timing issues and errors.

CFX input files that define the mesh, flow domain initialization, and boundary conditions were placed on the HPC drive. To triple the input files were produced, they were generated simultaneously on three computers: a quad-core desktop (host in Fig. 2.9) and two dual-core desktops (Peer1 and Peer2 in Fig. 2.9).

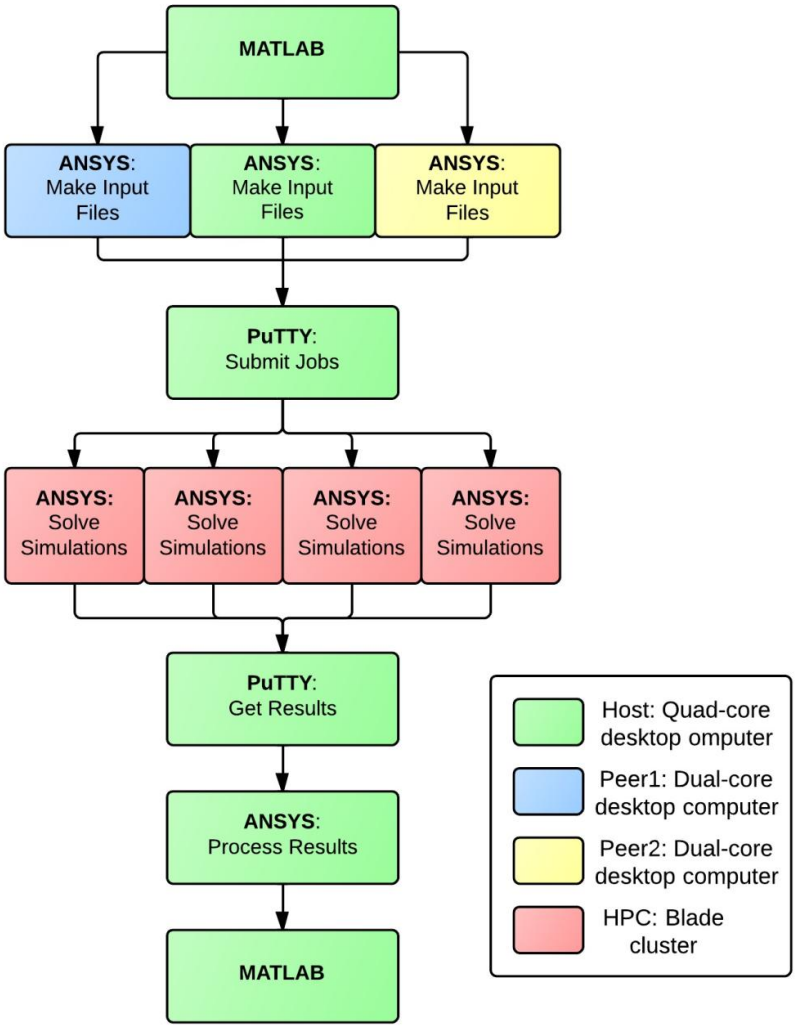

Figure 2.9: Flow chart for the design evaluation process using the HPC (colors indicate which system performed each task

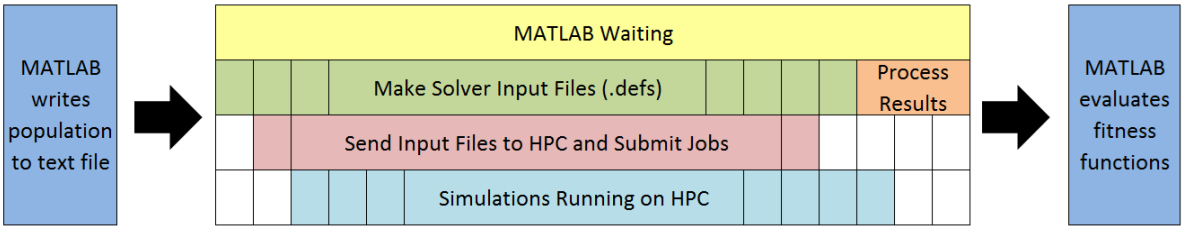

Figure 2.10: Gantt chart for design evaluation process emphasizing timing and parallelization (colors distinguish between tasks)

3 RESULTS

The MOGA converged after 100 generations (Fig. 3.1), which took twenty days using the HPC. The same optimization would have taken approximately 250 days on a single quad-core computer. The success of the optimization is demonstrated in Fig. 3.1, which shows the MOGA results approaching the theoretical performance limit (red curve in Fig. 3.1, described in Section 2.2.2).

Comparing the final Pareto frontier (Fig. 3.2) to the second generation prototype, it is clear that the optimization resulted in numerous designs with simultaneous improvements in both performance objectives. The region of the Pareto frontier that dominates the second generation prototype is the "hypervolume of dominating designs" (the term "hypervolume" is used in multi-objective optimization to compare two performance frontiers [29]). The two extreme designs of the Pareto curve are labeled Design 1 and Design 2, where Design 1 has the shortest pintle stroke and Design 2 has the smallest spray angle sensitivity. The objective function and design parameter values for Design 1, Design 2, and the second generation prototype are listed in Table 3.1, and these three designs are visually displayed in Fig. 3.3.

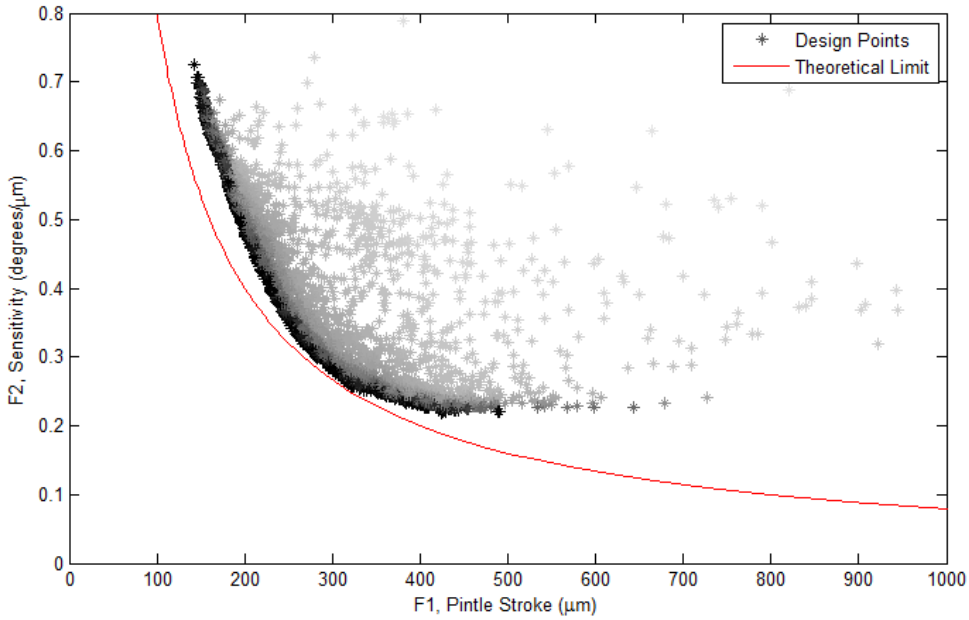

Figure 3.1: The VGS performance space; design point shading indicates generation number (light shades: early generations, dark shades: later generations), demonstrating convergence of the MOGA and resulting Pareto frontier. Red curve represents theoretical performance limit.

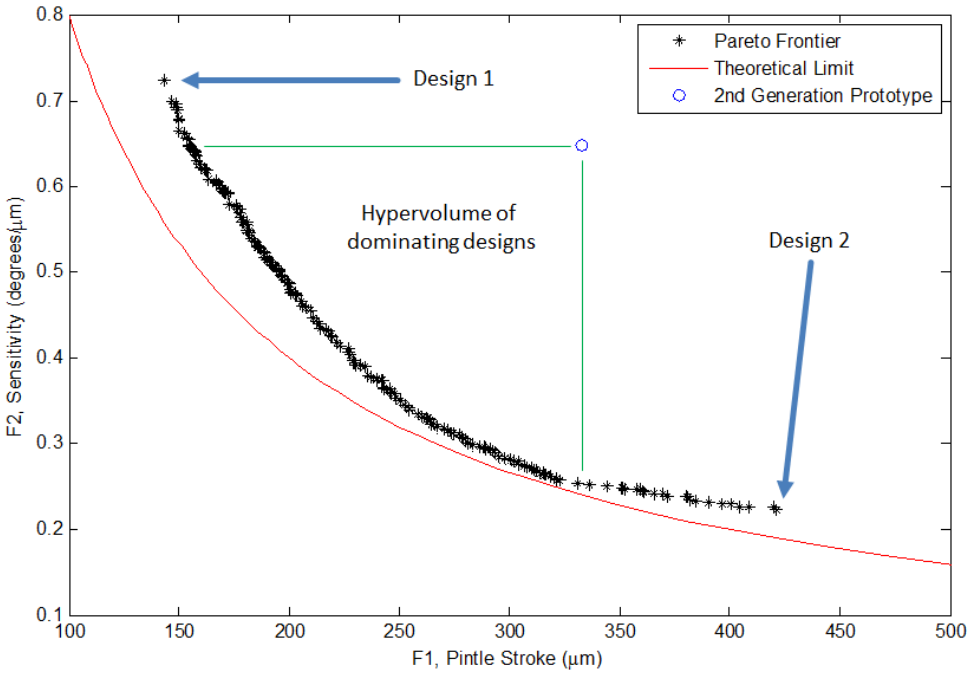

Figure 3.2: VGS performance space highlighting the final Pareto frontier and the second generation prototype, with extreme VGS designs annotated as Design 1 and Design 2.

Table 3.1: Optimized design parameters and objective functions for Design 1, Design 2, and the second generation prototype (Prototype 2)

	Objective Functions		Design Parameters					
Design	F_1 (μm)	F_2 (°/μm)	Major Pintle Diameter u_1 (mm)	Minor Pintle Diameter u_2 (mm)	Pintle Fillet u_3 (mm)	Nozzle Angle u_4 (°)	Orifice Fillet u_5 (mm)	Orifice Diameter u_6 (mm)
Prototype 2	340.6	0.647	1.500	0.729	0.254	150	0.000	1.700
Design 1	143.3	0.724	1.972	0.612	0.278	160.57	0.019	2.172
Design 2	421.2	0.223	1.632	0.640	0.104	172.15	0.300	1.832

Table 3.2: Correlation coefficients (ρ) between the design parameters and the objective functions

	Major Pintle Diameter u_1	Minor Pintle Diameter u_2	Pintle Fillet u_3	Nozzle Angle u_4	Orifice Fillet u_5	Orifice Diameter u_6
ρ_{F1} (pintle stroke)	-0.780	0.140	-0.799	-0.430	0.978	-0.780
ρ_{F2} (sensitivity)	0.457	-0.045	0.553	0.369	-0.745	0.457

Correlation coefficients were calculated for the Pareto frontier to analyze the dependencies between the design parameters and the objective functions (Table 3.2). Coefficients approaching +1.0 or -1.0 one indicate a strong dependency between a specific design parameter and objective function. It is clear that the orifice fillet has the greatest influence on the pintle stroke ($\rho_{F1\text{-}u5}$=0.978). The effects of the pintle fillet ($\rho_{F1\text{-}u3}$=-0.799), major pintle diameter ($\rho_{F1\text{-}u1}$=-0.780), and orifice diameter ($\rho_{F1\text{-}u6}$=-0.780) are significant, but not to the same degree as the orifice fillet. Note that the coefficients for the major pintle diameter ($\rho_{F1\text{-}u1}$ and $\rho_{F2\text{-}u1}$) and orifice diameter ($\rho_{F1\text{-}u6}$ and $\rho_{F2\text{-}u6}$) are equal because of the equality constraint imposed on these two design parameters. Finally, the orifice fillet has the greatest effect on the sensitivity ($\rho_{F1\text{-}u5}$=-0.745), and the pintle fillet has the second greatest

effect ($\rho_{F1\text{-}u3}$=0.553). This novel simulation-based design optimization strategy revealed and quantified these dependencies between the injector's physical geometry and spray angle characteristics that would be difficult or impossible to establish other ways.

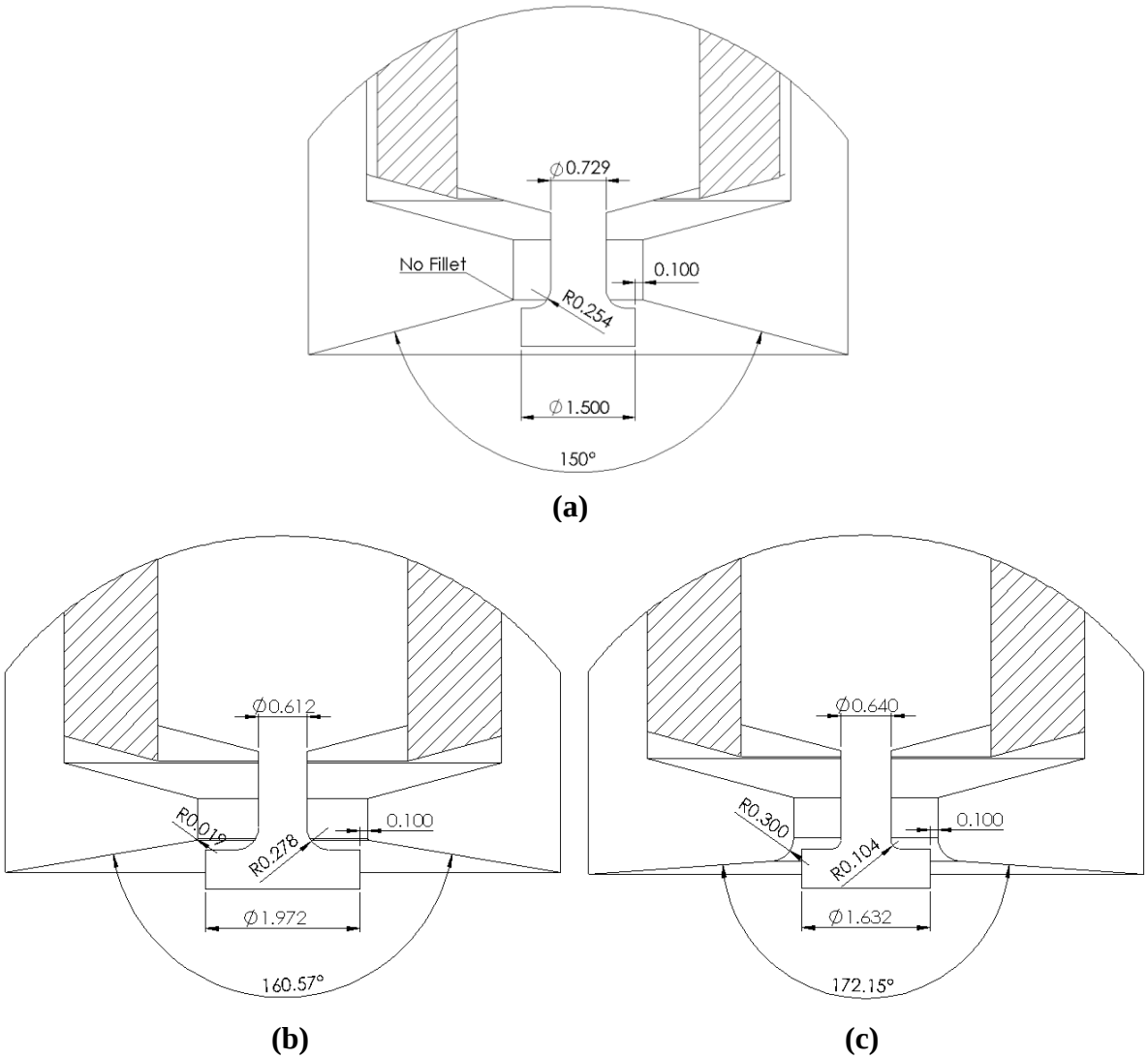

Figure 3.3: The design variables (VGS geometries) for (a) the second generation prototype, (b) Design 1, and (c) Design 2, showing how the design parameters varied in the optimization

The dependencies of spray angle on pintle position for these three designs (Fig. 3.4) were also examined to gain further insight into the performance space. The tradeoff between actuator stroke and spray angle sensitivity is clearly demonstrated by comparing the extreme designs of the Pareto curve: Design 2 has a much smaller slope (sensitivity) than Design 1, but it has a much greater actuator stroke. Fig. 25 also reveals that while the spray angles are nonlinear with respect to pintle position for all three designs, nonlinearities in Design 1 and Design 2 are greatly reduced within the desired range of spray angles (70-150°). It is important to note that within the pintle range evaluated in the MOGA, Design 2 does not reach the full desired range of spray angles. However, the nonlinear regression predicts that it will reach the desired spray angle of 150° as the pintle moves past 550μm.

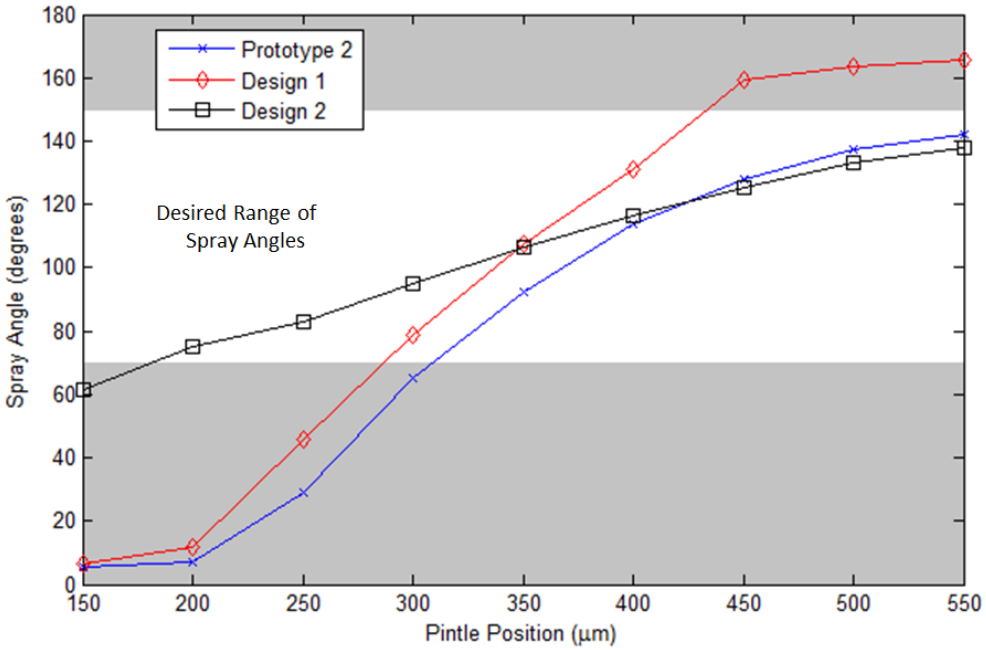

Figure 3.4: Graph of spray angle versus pintle position for Design 1, Design 2, and the second generation prototype (Prototype 2), demonstrating the tradeoff between the performance objectives

Two limitations of this optimization approach should be addressed. First, the droplet size requirement was enforced by fixing the annular gap at 100μm (section 1.2), removing one degree of freedom from the design space. Overcoming this limitation in future research could lead to further performance improvements on the Pareto frontier. Second, the MOGA provides a frontier of possible solution points, but does not determine any single design that is optimal from that group. It provided the designers with a performance tradeoff curve to make informed decisions about the geometry of future VGS prototypes.

4 CONCLUSION

This paper demonstrates a novel method for using optimization tools interfaced to state-of-the-art computational tools to efficiently find optimal design geometries in a complex design space with multiple performance objectives. The MOGA, which navigated the design space for optimality, was interfaced to cutting edge CFD analysis software to evaluate candidate VGS designs. The CFD model was validated by comparison to empirically measured spray test results from prior prototypes. Due to the high computational cost to evaluate candidate designs, a high performance computing cluster was employed to evaluate as many as 20 designs at once, dramatically reducing functional evaluation time.

The MOGA found a Pareto frontier that accurately represents the tradeoff between the two performance objectives. This Pareto frontier demonstrates significant opportunity for performance improvements because it dominates the second generation prototype. By examining two design cases at the extremes of the Pareto frontier, critical relationships between the design parameters and the performance objectives were identified.

Future work should focus on the fabrication and testing of extreme Pareto designs (Design 1 and Design 2) to verify the optimization results and demonstrate the improved control and actuation of the injector. Additional work could integrate a more powerful CFD tool, namely KIVA, a family of CFD software developed by Los Alamos National Laboratory to predict fuel and air flows as well as ignition and combustion processes [30]. Using KIVA, the droplet size constraints could be computationally evaluated, adding an additional degree of freedom to the design space by removing the need for a geometric equality constraint. Finally, the optimization could be run with additional performance objectives such as droplet size, combustion performance, and material cost to investigate other important design considerations.

REFERENCES

[1] *Federal Register*, 66:5002-5193, 2001.

[2] T. Kaminoto and M. Bae. High combustion temperature for the reduction of particulate in diesel engines. *SAE transactions*, 97:692-701, 1989.

[3] J.E. Dec. Advanced compression-ignition engines-understanding the in-cylinder processes. *Proceedings of the Combustion Institute*, 32(2):2727-2742, 2009.

[4] Mingfa Yao, Zhaolei Zheng, and Haifeng Liu. Progress and recent trends in homogeneous charge compression ignition (hcci) engines. *Progress in Energy and Combustion Science*, 35:398-437, 2009.

[5] Magnus Christensen. HCCI Combustion-Engine Operation and Emission Characteristics. PhD thesis, Lund University, 2002.

[6] Bertrand Gatellier, Bruno Walter, and Marjorie Miche. New diesel combustion process to achieve near zero NO_x and particulates emissions. *A new generation of engine combustion processes for the future?*, pp. 43-52. Editions Technip, Paris, 2001.

[7] Kevin Duffy. Heavy truck clean diesel (htcd) program. *Diesel Engine Emission Reduction Conference*, 2004.

[8] Yong Sun and Rolf D. Reitz. Modeling diesel engine nox and soot reduction with optimized two-stage combustion. *SAE 2006 World Congress & Exhibition*, April 2006. SAE Paper 2006-01-0027.

[9] Tiegang Fang, Robert E. Coverdill, Chia fon F. Lee, and Robert A. White. Effects of injection angles on combustion processes using multiple injection strategies in an hsdi diesel engine. *Fuel*, 87:3232-3239, 2008.

[10] J.P. Lien. Design, Modeling, and Control of a Variable Geometry Spray Fuel Injector. PhD thesis, North Carolina State University, 2011. `

[11] J.P. Lien, Ji Zhang, T. Fang, and G. Buckner. *International Conference on Liquid Atomization and Spray Systems*, 2011.

[12] Niebrzydoski, John. 1995. Fuel injection system for internal combustion engines. U.S. Patent 5,398,654, filed April 4, 1994, and issued March 21, 1995.

[13] Malvern Instruments Ltd. Spraytec, MAL 1009475. Worcestershire, United Kingdom, 2006.

[14] J. Yang, E.W. Kaiser, W.O. Siegl, and R.W. Anderson. Effects of port-injection timing and fuel droplet size on total and speciated exhaust hydrocarbon emissions. *SAE Transactions*, 1993.

[15] Kastengren, A.L., Tilocco, F.Z., Powell, C.F., Manin, J., Pickett, L.M., Payri, R., and Bazyn, T., "Engine Combustion Network (ECN): Measurements of Nozzle Diameter and Hydraulic Behavior of Diesel Sprays," Atomization and Sprays, submitted 2012.

[16] J.R. Archer, J.P. Lien, T. Fang, and G. Buckner. *International Conference on Liquid Atomization and Spray Systems*, 2012.

[17] Fujii, Hiroto. 2007. Injector for high-pressure injection. U.S. Patent 7,222,608, filed

September 1, 2005, and issue May 29, 2007.

[18] ANSYS, Inc. ANSYS Workbench 12.0, Canonsburg, Pennsylvania, 2008.

[19] A. W. Date *Introduction to Computational Fluid Dynamics*. Cambridge University Press, New York: (2005).

[20] J. Crews, M Mattson, G. Buckner, Multi-objective control optimization for semi-active vehicle suspensions, *Journal of Sound and Vibration*, 330 (2011) 5502-5516.

[21] M. Srinivas, L. Patnaik, Genetic algorithms: a survey, *IEEE Computer* 27 (6) (1994) 17–26.

[22] S. Rajeev, C.S. Krishnamoorthy, Genetic algorithms-based methodologies for design optimization of trusses, *Journal of Structural Engineering* 123 (3) (1997) 350–358.

[23] A.E. Baumal, J.J. McPhee, P.H. Calamai, Application of genetic algorithms to the design optimization of an active vehicle suspension system, *Computer Methods in Applied Mechanics and Engineering* 163 (1998)87–94.

[24] R. Dimeo, K.Lee, Boiler-turbine control system design using a genetic algorithm, *IEEE Transactions on Energy Conversion* 10 (4) (1995) 752–759.

[25] Z. Michalewicz, C. Janiko, J. Krawczjk, A modified genetic algorithm for optimal control problems, *Computers and Mathematics with Applications* 23 (2) (1992) 83–94.

[26] C.M. Fonseca, P.J. Fleming, Genetic algorithms for multiobjective optimization: Formulation, discussion, and generalization, in: S. Forest (Ed.), *Proceedings from the Fifth International Conference on Genetic Algorithms*, San Mateo, CA, 1993, pp.416–423.

[27] K. Deb, Multi-objective genetic algorithms: problem difficulties and construction of test problems, *Evolutionary Computation* 7 (3)(1999)205–230.

[28] A. Suleman, E. Prasad, R. Blackow, and D. Waechter. Smart structres – an overview. In A. Suleman, editor, Smart Structures: Applications and Related Technologies, number 429 in CISM Courses and Lectures. Springer, 2001.

[29] N. Beume, B. Naujoks, M. Emmerich, SMS-EMOA: Multiobjective selection based on dominated hypervolume, *European Journal of Operational Research* 181 (3) (2007) 1653-1669.

[30] Los Alamos National Laboratory. KIVA, Los Alamos, NM, 2010.